

# Stress Analysis of Adhesive Bonded Joints Under In-Plane Shear Loading

Hyonny Kim\* and Keith T. Kedward

*Department of Mechanical and Environmental Engineering  
University of California, Santa Barbara, CA 93106, USA*

A closed-form stress analysis of an adhesive bonded lap joint subjected to spatially varying in-plane shear loading is presented. The solution, while similar to Volkersen's treatment of tension loaded lap joints, is inherently two-dimensional, and in general predicts a multi-component adhesive shear stress state. A finite difference numerical solution of the derived governing differential equation is used to verify the accuracy of the closed-form solution for a joint of semi-infinite geometry. The stress analysis of a finite sized doubler is also presented. This analysis predicts the adhesive stresses at the doubler boundaries, and can be performed independently from the complex stress state that would exist due to a patched crack or hole located within the interior of the doubler. The analytical treatment of lap joints under combined tension and shear loading is now simplified since superposition principles allow the stress states predicted by separate shear and tension cases to be added together. Applications and joint geometries are discussed.

**Keywords:** shear-load, bonded joint, doubler, composite adherend, crack patch, closed-form analysis

## Nomenclature

$x, y, z$	Rectangular coordinates
$r, \theta, s$	Cylindrical and shell coordinates
$2c$	Overlap length of adhesive joint
$a$	Width of joint over which applied loading varies, or length of doubler in $x$ -direction
$b$	Length of doubler in $y$ -direction
$t_i, t_o$	Thickness of inner, outer adherend

---

\* corresponding author

$t_a$	Thickness of adhesive layer
$E_y^i, E_y^o$	Young's modulus of inner, outer adherend in the $y$ -direction
$G_{xy}^i, G_{xy}^o$	Shear modulus of inner, outer adherend
$G_a$	Shear modulus of adhesive layer
$N_x, N_y$	Applied direct stress resultants (force per unit width)
$N_{xy}$	Applied shear stress resultant (force per unit width)
$\sigma_y^i, \sigma_y^o$	Direct stress in inner, outer adherend in the $y$ -direction
$\tau_{xy}^i, \tau_{xy}^o$	Shear stress in inner, outer adherend
$\gamma_{xy}^i, \gamma_{xy}^o$	Shear strain in inner, outer adherend
$\tau_{xz}^a, \tau_{yz}^a$	Adhesive shear stress components acting in $x$ - $z$ , $y$ - $z$ plane
$\gamma_{xz}^a, \gamma_{yz}^a$	Adhesive shear strain components acting in $x$ - $z$ , $y$ - $z$ plane
$u_i, u_o$	Displacement of inner, outer adherend in $x$ -direction
$v_i, v_o$	Displacement of inner, outer adherend in $y$ -direction

## 1. Introduction

Adhesive bonding has been applied successfully in many technologies. Foremost in applications where primary loaded structures rely on adhesive bonding are aircraft and space structures.

While bonding in large and small commercial aircraft has been practiced quite widely in Europe (sailplanes in Germany, SAAB 340 [1], and EXTRA EA-400 [2]), extensive adhesive bonding is being used in the United States for the assembly of newly emerging small all-composite aircraft structures (Cirrus SR20 and Lancair Columbia 300) for reasons related to performance and cost.

The analytical treatment of a bonded lap joint where the adherends are loaded in tension (see Figure 1) has been considered extensively by many authors. Hart-Smith [3, 4] extended the shear lag theory that was presented by Volkersen [5] to include adhesive plasticity. Goland and Reissner [6] and Oplinger [7] accounted for adherend bending deflections to predict the peel stress in the adhesive. Tsai, Oplinger, and Morton [8] provided a correction for adherend shear deformation, resulting in a simple modification of the Volkersen's theory based equations. All of

these analytical treatments are formulated per unit width of the specimen which implies that the predicted adhesive stress is independent of variations of loading through the width of the joint ( $x$ -direction in Figure 1). An extension of these solutions can be applied to the case of spatially varying tensile loading, as shown in Figure 1, by performing the analysis using the value of tensile stress resultant at any particular  $x$ -axis location. The tension loaded lap joint analysis is presented in Appendix A.

Adhesively bonded lap geometries loaded by in-plane shear (see Figure 2) have been discussed by Hart-Smith [4], van Rijn [2], and the Engineering Sciences Data Unit [9]. The authors of these works indicate that shear loading can be analytically accounted for by simply replacing the adherend Young's moduli in the tensile loaded lap joint solution with the respective adherend shear moduli. This approach is rigorously correct for only the case of spatially constant  $N_{xy}$  load applied to joints which are semi-infinite, as shown in Figure 2a.

When the geometry is finite in size (see Figure 2b), an analytical treatment that is more comprehensive than that suggested by Hart-Smith [4], van Rijn [2], and the Engineering Sciences Data Unit [9] is needed in order to account for adhesive stresses which would exist at the bond terminations. Thus the objective of the theoretical work presented herein is to address the shear loaded lap joint problem in more general terms by allowing the applied in-plane shear load to vary in the spatial coordinates, and by accounting for a joint geometry of finite size. Closed-form analytical solutions are developed for single and double lap joint configurations subject to general in-plane shear loading. It should be noted that the solution of this problem using Finite Element Analysis (FEA) is difficult due to the inherent three-dimensional nature of the joint geometry and shear loading conditions. Since three-dimensional elements need to be

used in modeling shear transfer across a lap joint, creating a mesh having enough element refinement to capture the high stress gradients in the thin adhesive layer can easily result in a FEA model of formidable size. In comparison, a closed-form solution to this problem serves as a computationally efficient tool that is useful for design and analysis.

## **2. Structural Examples**

Examples of structures in which shear loading can challenge a bonded lap joint are shown in Figures 3 to 7. Figure 3 shows a generic section of an adhesive bonded fuselage assembly typical of small aircraft. The fuselage halves are joined at the fuselage centerline, typically through a joggled lap joint, as shown in the figure inset. Other joint configurations might include the use of a splice strap. Shear loads are transmitted by this joint any time torsion is carried by the fuselage, such as when the aircraft rudder is used during maneuvers or when side gusts load the tail. Note that the fuselage cross-section decreases in moving aft, so that for a given applied torque load at the tail, the shear stress in the fuselage skin increases in the direction of shrinking cross-section. Also detailed in Figure 3 is a bonded joint connecting an internal shelf structure to the outer fuselage shell. When the fuselage skin carries torsion, shear flow is introduced into the shelf through the bonded clips, in the manner of a two-cell torsion box. Finally, a bonded doubler is pointed out in Figure 3. Doublers are used where a local increase in wall thickness is needed, such as for attaching an antenna or carrying a concentrated load. This doubler could potentially debond when significant loads are carried by the fuselage skin.

The joining of tubular structures is another case in which shear loading is applied across a lap joint. The circumferential joint under torsion loading, shown in Figure 4a has been treated analytically by Adams and Peppiat [10]. For the circumferential joint orientation, the analysis is

one-dimensional, i.e. adhesive stress is independent of circumferential position. The theory presented in this paper applies to the circumferential joint case for thin-walled structures. This thin-walled condition implies that the torsion-induced shear stress in the adherend has negligible through thickness variation. Additionally, the theory presented herein is applicable to the thin-walled longitudinal joint geometry as shown in Figure 4b. This structure can be subjected to an axially varying running torque or end-applied torque. Both the circumferential and longitudinal joint geometry can be found in aircraft structures, such as the large transport aircraft fuselage barrel studied under the Primary Adhesively Bonded Structure Technology (PABST) program [1].

Another torsion-loaded geometry, shown in Figure 5, is a face-bonded circular lap joint. Here torque load is transferred through an interface plate to an outer circular plate. This geometry results in an axisymmetric adhesive stress profile. Note that the shear stress resultant transmitted through the joint,  $N_{r\theta}$ , is dependent upon the radius,  $r$ .

Figure 6 depicts a wing box of generic construction [11] using bonded angle clips to hold shear webs in place. When the wing is subjected to aerodynamic lift loads and torsion during maneuvers, shear stresses are introduced into the shear webs through the bonded angle clips. Observe in the figure that the regions where the clips are bonded to the shear webs are essentially double lap joints. This structure can be idealized as a bonded-construction I-beam carrying pressure load, as shown in Figure 7. Simple structural analysis treatments are available [11, 12] to determine the shear load transferred through cut A-A in the figure for use in a subsequent bonded joint analysis. For a uniform pressure load acting along the length of a constant cross-section beam, as in Figure 7, the shear load in the web varies linearly along the width of the joint

(i.e. along the length of the beam). Large cutouts in the shear web and concentrated point loads applied along the length of the beam would introduce sharp variations in the shear loading carried by the clips. The theory presented in this paper is capable of accounting for these variations.

### 3. Governing Equation

The derivation of the differential equation governing the behavior of a shear loaded adhesive joint is presented in this section. While analogous to the tension loaded case which results in a one-dimensional ordinary differential equation, the end result for the shear case is a two-dimensional partial differential equation.

Consider the shear loaded bonded lap joint shown in Figure 8. The differential element in Figure 8 shows the in-plane shear stresses acting on the inner and outer adherends,  $\tau_{xy}^i$  and  $\tau_{xy}^o$ , as well as the two components of adhesive shear stress,  $\tau_{xz}^a$  and  $\tau_{yz}^a$ . This analysis is applicable to both the single and double lap joint geometries which are illustrated in Figure 9. The double lap case is limited to the condition of geometric and material symmetry about the center of the inner adherend, so that the problem is then identical to the single lap case. Alternatively, if both outer adherends have equivalent stiffness, i.e. same product of shear modulus and thickness, then the double lap joint can still be treated as symmetric. Assumptions made in the derivation are:

1. Constant bond and adherend thickness.
2. Uniform distribution of shear strain through the adhesive thickness.
3. Adhesive carries only out-of-plane stresses while adherends carry only in-plane stresses.
4. Linear elastic material behavior.
5. Deformation of the adherends in the out-of-plane direction is negligible.

The lap-jointed shear panel, shown in Figure 8, has an applied shear stress resultant  $N_{xy}$  which is continuous through the overlap region, and at any point must equal the sum of the product of each adherend shear stress with its respective thickness.

$$N_{xy} = \tau_{xy}^i t_i + \tau_{xy}^o t_o \quad (1)$$

Force equilibrium performed on a differential element of the outer adherend, shown in Figure 10, results in relationships between the adhesive stress components and the outer adherend shear stress.

$$\begin{aligned} \Sigma F_x &= -\tau_{xy}^o t_o dx + \left( \tau_{xy}^o + \frac{\partial \tau_{xy}^o}{\partial y} dy \right) t_o dx - \tau_{xz}^a dx dy = 0 \\ \tau_{xz}^a &= t_o \frac{\partial \tau_{xy}^o}{\partial y} \end{aligned} \quad (2)$$

$$\begin{aligned} \Sigma F_y &= -\tau_{xy}^o t_o dy + \left( \tau_{xy}^o + \frac{\partial \tau_{xy}^o}{\partial x} dx \right) t_o dy - \tau_{yz}^a dx dy = 0 \\ \tau_{yz}^a &= t_o \frac{\partial \tau_{xy}^o}{\partial x} \end{aligned} \quad (3)$$

The adhesive shear strains are written based on the assumption of constant shear strain across the thickness of the adhesive.

$$\gamma_{xz}^a = \frac{\tau_{xz}^a}{G_a} = \frac{1}{t_a} (u_o - u_i) \quad \text{and} \quad \gamma_{yz}^a = \frac{\tau_{yz}^a}{G_a} = \frac{1}{t_a} (v_o - v_i) \quad (4) \text{ and } (5)$$

Taking the  $y$ - and  $x$ -derivatives of  $\gamma_{xz}^a$  and  $\gamma_{yz}^a$ , respectively,

$$\frac{\partial \gamma_{xz}^a}{\partial y} = \frac{\partial \tau_{xz}^a}{G_a \partial y} = \frac{1}{t_a} \left( \frac{\partial u_o}{\partial y} - \frac{\partial u_i}{\partial y} \right) \quad (6)$$

$$\frac{\partial \gamma_{yz}^a}{\partial x} = \frac{\partial \tau_{yz}^a}{G_a \partial x} = \frac{1}{t_a} \left( \frac{\partial v_o}{\partial x} - \frac{\partial v_i}{\partial x} \right) \quad (7)$$

Adding the resulting equations, (6) and (7), one gets

$$\frac{\partial \tau_{xz}^a}{\partial y} + \frac{\partial \tau_{yz}^a}{\partial x} = \frac{G_a}{t_a} \left( \frac{\partial u_o}{\partial y} + \frac{\partial v_o}{\partial x} - \frac{\partial u_i}{\partial y} - \frac{\partial v_i}{\partial x} \right) \quad (8)$$

Finally, combining equation (8) with equations (1) to (3), and noting that

$$\frac{\partial u_o}{\partial y} + \frac{\partial v_o}{\partial x} = \gamma_{xy}^o = \frac{\tau_{xy}^o}{G_{xy}^o} \quad \text{and} \quad \frac{\partial u_i}{\partial y} + \frac{\partial v_i}{\partial x} = \gamma_{xy}^i = \frac{\tau_{xy}^i}{G_{xy}^i} \quad (9) \text{ and } (10)$$

results in a partial differential equation governing the shear stress in the outer adherend.

$$\nabla^2 \tau_{xy}^o - \lambda^2 \tau_{xy}^o + C_o = 0 \quad (11)$$

$$\text{with } \lambda^2 = \frac{G_a}{t_a} \left( \frac{1}{G_{xy}^o t_o} + \frac{1}{G_{xy}^i t_i} \right) \quad \text{and} \quad C_o = \frac{G_a N_{xy}}{G_{xy}^i t_a t_i t_o} \quad (12) \text{ and } (13)$$

The adhesive shear stresses  $\tau_{xz}^a$  and  $\tau_{yz}^a$  can be obtained from the relationships given by equations (2) and (3) once a solution to equation (11) is determined. The governing equation is similar to the one-dimensional equation governing the behavior of a tension loaded bonded joint (see Appendix A). Note however that for the shear loaded case, the governing equation is in two dimensions, and there are now, in general, two components of adhesive shear stress.

This derivation is rigorously correct for the case when the applied loading,  $N_{xy}$ , is constant with respect to the  $x$ - and  $y$ -coordinates. For the case when  $N_{xy}$  has gradients in the  $x$ - and  $y$ -directions, there will generally exist complementary direct stress resultants,  $N_x$  and  $N_y$ , with gradients in the  $x$ - and  $y$ -directions, respectively. This point is clear when considering the equilibrium equations of a flat plate

$$\frac{\partial N_x}{\partial x} + \frac{\partial N_{xy}}{\partial y} = -q_x \quad (14)$$

$$\frac{\partial N_{xy}}{\partial x} + \frac{\partial N_y}{\partial y} = -q_y \quad (15)$$

where applied surface tractions  $q_x$  and  $q_y$  are zero. For example, equation (15) says that for  $N_{xy}$  being a function behaving linearly in  $x$ , in order for equilibrium to be maintained,  $N_y$  must be linear in  $y$  (for  $q_y = 0$ ). The existence of these additional stress resultants, not accounted for in the derivation of equation (11), will contribute additional stresses in the adhesive. For many engineering structures, such as the shear webs shown in Figures 6 and 7, the gradients of  $N_{xy}$  in the shear web are small enough so that the influence of these equilibrium-maintaining stress resultants,  $N_x$  and  $N_y$ , on the derivation of the governing equation can often be neglected. If the magnitude of  $N_x$  and  $N_y$  are too great to be treated as negligible, their effect can be accounted for through a separate tension (or compression) loaded bonded joint analysis (see Appendix A). The results of this analysis can then be superposed onto the results of the shear-loaded joint analysis.

Cases where a gradient in  $N_{xy}$  can exist without complementary  $N_x$  or  $N_y$  resultants can be found in flat structures having surface tractions  $q_x$  and  $q_y$  present, and in torsion-loaded thin-walled structures of varying closed cross-section, such as the generic fuselage depicted in Figure 3. In this example, the structure can be idealized as conical shell, as illustrated in Figure 11. For an applied end-torque, the shear flow in the wall,  $N_{s\theta}$ , will vary along the meridional direction,  $s$ , solely due to the effects of changing cross-section geometry.

$$N_{s\theta} = \frac{T}{2\pi r^2} = \frac{T}{2\pi s^2 \cos^2 \alpha} \quad (16)$$

The existence of an equilibrium-maintaining hoop stress is not necessary in this case, as can be confirmed by inserting equation (16) into the  $\theta$ -direction equilibrium equation for a conical shell [13] with no surface tractions or body forces present.

$$\frac{\partial(sN_{s\theta})}{\partial s} + \frac{\partial N_{\theta}}{\partial \theta} \frac{1}{\cos \alpha} + N_{s\theta} = 0 \quad (17)$$

#### 4. Solution for Semi-Infinite Case

This section presents the solution to the governing equation (11) for the case of a semi-infinite joint. This type of joint does not consider the termination of the joint in the width, or  $x$ -direction (see Figure 2a), and is oriented such that the length of the joint,  $2c$ , runs parallel to the  $y$ -axis coordinate.

A closed-form solution is obtained for the condition in which the loading  $N_{xy}$  smoothly varies in the  $x$ -direction. An example of this type of loading condition is depicted in Figure 12. Since the governing equation has been formulated using differential scale elements, the assumption is made that the smoothly varying load  $N_{xy}$  can be locally represented as a linear function in  $x$  (e.g. by using a Taylor Series expansion). After obtaining the solution, this linear assumption is relaxed, and the resulting closed-form expressions will be shown, through comparison with a numerical calculation, to remain valid for non-linear functions as well.

Applying the assumption that  $N_{xy}$  is represented by a linear function in the  $x$ -direction, and furthermore  $N_{xy}$  is also constant in the  $y$ -direction, a solution to equation (11), having form identical to that of Volkersen's one-dimensional tension-loaded case can be assumed.

$$\tau_{xy}^o = A_o \cosh \lambda y + B_o \sinh \lambda y + \frac{C_o}{\lambda^2} \quad (18)$$

where  $\lambda^2$  and  $C_o$  are given by equations (12) and (13). Note that  $C_o$  is directly proportional to  $N_{xy}$  and is thus considered to be linear in  $x$ .  $A_o$  and  $B_o$  are unknown terms which can be functions of  $x$ , and it is assumed that, like  $C_o$ , they are no higher than linear functions in  $x$ . The solution obtained will confirm this assumption by showing  $A_o$  and  $B_o$  to be directly proportional to  $N_{xy}$ . Substituting equation (18) into the governing equation (11) checks that this is a valid solution.

Using the following boundary conditions (see joint geometry in Figure 9),

$$\tau_{xy}^o = 0 \text{ at } y = -c \quad (19)$$

$$\tau_{xy}^o = \frac{N_{xy}}{t_o} \text{ at } y = c \quad (20)$$

the unknown terms can be determined.

$$A_o = \frac{1}{\cosh \lambda c} \left( \frac{N_{xy}}{2t_o} - \frac{C_o}{\lambda^2} \right) \quad (21)$$

$$B_o = \frac{N_{xy}}{2t_o \sinh \lambda c} \quad (22)$$

The adhesive shear stress components can now be calculated using equations (2), (3) and (18).

$$\tau_{xz}^a = t_o \frac{\partial \tau_{xy}^o}{\partial y} = t_o \lambda (A_o \sinh \lambda y + B_o \cosh \lambda y) \quad (23)$$

$$\left( \tau_{yz}^a \right)_{N_{xy}} = t_o \frac{\partial \tau_{xy}^o}{\partial x} = t_o \left( \frac{\partial A_o}{\partial x} \cosh \lambda y + \frac{\partial B_o}{\partial x} \sinh \lambda y + \frac{1}{\lambda^2} \frac{\partial C_o}{\partial x} \right) \quad (24)$$

For the case of constant  $N_{xy}$ , the stress component  $\left( \tau_{yz}^a \right)_{N_{xy}}$  is zero since  $A_o$ ,  $B_o$ , and  $C_o$  would be constants. For a smooth  $x$ -varying load function  $N_{xy}(x)$ , the stress component  $\tau_{xz}^a$  simply varies in direct proportion to the loading, while equation (24) calculates a non-zero adhesive stress component  $\left( \tau_{yz}^a \right)_{N_{xy}}$  to exist in order to satisfy force equilibrium in the  $y$ -direction. This however is an incomplete result since it does not account for the previously discussed equilibrium-maintaining stress resultant  $N_y$  that would exist for flat plate structures having  $\partial N_{xy} / \partial x \neq 0$ . The  $N_y$  stress resultant not only maintains force equilibrium in the  $y$ -direction, but also produces an adhesive stress  $\left( \tau_{yz}^a \right)_{N_y}$ . Therefore, in order to completely calculate the  $\tau_{yz}^a$  adhesive stress, both contributions arising from the gradient in  $N_{xy}$  and the presence of  $N_y$  must be added together.

$$\tau_{yz}^a = (\tau_{yz}^a)_{N_{xy}} + (\tau_{yz}^a)_{N_y} \quad (25)$$

In many engineering structures, the  $N_y$  stress resultant magnitude is small when compared with the  $N_{xy}$  loads, resulting in the  $\tau_{yz}^a$  stress component being generally much smaller than  $\tau_{xz}^a$ .

Finally, note that analytical solutions for the semi-infinite bonded joint can also be determined for the case of  $y$ -varying  $N_{xy}$  loading. Equation (18) is the general solution when  $N_{xy}$  is independent of  $y$ . By assuming that  $N_{xy}$  has at most a linear relationship in  $x$ , the governing equation (11) can be treated as an ordinary differential equation with independent variable  $y$ . The *Method of Undetermined Coefficients* [14] can be used to formulate the solution for certain cases where  $N_{xy}$  has a functional dependence of on the  $y$ -coordinate. This solution is summarized in Appendix B.

### Example and Validation by Finite Difference

The closed-form solution developed for a semi-infinite joint is now demonstrated for the example of a bonded I-beam shear web, as illustrated in Figure 12. A particular interest exists to test the solution for a shear load  $N_{xy}(x)$  that is arbitrary and smoothly varying (i.e. not a linear function of  $x$ ). To this end, a shear loading function is chosen to represent the transition in shear flow in the web in the region adjacent to an applied point load, as shown in Figure 12.

$$N_{xy} = 4.38 \left( \cos \frac{\pi x}{a} + 3 \right) \text{ N/mm} \quad (26)$$

This function is valid in the width-direction of the joint in the region  $0 < x < a$  and is constant in the  $y$ -direction. For  $x < 0$ ,  $N_{xy}$  is constant at 17.5 N/mm, and for  $x > a$ ,  $N_{xy}$  is constant at 8.75 N/mm. The calculation is performed using the same joint geometry for two laminated composite

adherend cases: (i) woven glass/epoxy, and (ii) unidirectional standard modulus carbon/epoxy. Both of these symmetrically laminated composite adherends have a  $\pm 45^\circ$  ply orientation content of 50%, with the remainder of the plies oriented at  $0^\circ$  and  $90^\circ$  in equal proportion (25% each). Furthermore, the thickness and material of both the inner and outer adherends are the same. This condition is a special case where the stiffness of the inner and outer adherends are the same. A joint with matching adherend stiffness is referred to as a *balanced joint*. Since stiffness is computed as the product of modulus and thickness, it is conceivable that a composite joint can be balanced with respect to shear loading, but not balanced with respect to tension or compression loading.

The geometry of the joint and the material properties of the adherends and adhesive are given in Table I.

Table I. Semi-Infinite Joint Geometry and Material Properties

Joint Parameter	Symbol	Value
length of bond overlap	$2c$	12.7 mm
joint width over which loading varies	$a$	25.4 mm
inner and outer adherend thickness	$t_i, t_o$	2.54 mm
adhesive thickness	$t_a$	0.254 mm
adhesive shear modulus	$G_a$	1.1 GPa
glass/epoxy laminate effective shear modulus (case 1)	$G_{xy}^i, G_{xy}^o$	6.5 GPa
glass/epoxy laminate effective tensile modulus (case 1)	$E_y^i, E_y^o$	17.2 GPa
carbon/epoxy laminate effective shear modulus (case 2)	$G_{xy}^i, G_{xy}^o$	21.4 GPa
carbon/epoxy laminate effective tensile modulus (case 2)	$E_y^i, E_y^o$	82.7 GPa

The  $\tau_{xy}^o$  stress in the outer adherend and the  $\tau_{xz}^a$  adhesive stress are calculated using the closed-form solution given by equations (18) and (21) to (23). These results are compared to a finite difference numerical solution of the governing equation (11). The finite difference model was

constructed to represent the outer adherend in the region of the bond overlap and over which the loading varied ( $-c < y < c$ ,  $0 < x < a$ ). The grid spacing was 0.508 mm in the  $x$ -direction, and 0.127 mm in the  $y$ -direction. The finer spacing in the  $y$ -direction is necessary to capture the high stress gradients existing along this direction, particularly at the termination of the joint overlap, at  $y = \pm c$ .

For the materials and geometry given in Table I, the adherend and adhesive stresses are computed, and normalized by a running average shear stress (i.e. average depends on  $x$ -position). The average shear stress in the outer adherend can be calculated by recognizing that each adherend carries a proportion of the applied load which is dependent upon the stiffness of the outer adherend relative to the inner.

$$\left(\tau_{xy}^o\right)_{ave} = \frac{G_{xy}^o N_{xy}}{G_{xy}^o t_o + G_{xy}^i t_i} \quad (27)$$

The average inner adherend shear stress can be calculated by replacing  $G_{xy}^o$  in the numerator of equation (27) with  $G_{xy}^i$ . The average adhesive shear stress acting in the  $x$ - $z$  direction is simply the shear load transferred across the joint divided by the overlap length.

$$\left(\tau_{xz}^a\right)_{ave} = \frac{N_{xy}}{2c} \quad (28)$$

The normalized adherend and adhesive shear stress profiles are shown in Figures 13 and 14 for both the glass/epoxy and carbon/epoxy adherend cases. In these figures, the closed-form solution is referred to by the abbreviation *CF*, and the finite difference results by *FD*. The stresses are plotted along the path  $x = 0.2a$ , which is a location away from a region of near constant applied loading (e.g.  $x = 0$ ), and for which the loading function is nonlinear in  $x$  (i.e.  $\partial^2 N_{xy} / \partial x^2 \neq 0$ ).

These criteria were used to select the location for solution comparison in order to demonstrate that the solution developed is valid for any general, smooth,  $x$ -varying load function.

Figures 13 and 14 show that the closed-form solution is nearly identical to the finite difference results. Note the different rate of load transfer between the two joint materials. The carbon/epoxy adherend has a significantly higher shear modulus, resulting in a more gradual transfer of shear loading between the two adherends (see Figure 13). The shear stress in the inner adherend,  $\tau_{xy}^i$ , can be obtained from equation (1) once the outer adherend stress  $\tau_{xy}^o$  is known. For a balanced joint, the inner adherend shear stress is simply a mirror image of Figure 13 about the  $y = 0$  axis.

The adhesive shear stress  $\tau_{xz}^a$ , shown in Figure 14, is a maximum at the edges of the joint at  $y = \pm c$ . This figure shows that a joint of identical geometry with more compliant (glass/epoxy) adherends results in significantly higher shear stress peaks. Conversely, a joint with stiffer adherends (carbon/epoxy) carrying the same loads has a higher minimum stress at the center of the overlap, and may need to be designed with a greater overlap length so as to maintain a low stress “elastic trough” that is long enough to avoid creep [15] in the adhesive. In joint design, it is necessary to address both the maximum and minimum stress levels in the adhesive, the former to avoid initial (short term) failures near the joint extremities, the latter to resist viscoelastic strain development under long term loading. For an unbalanced joint (e.g.  $t_o = 1.5$  mm), one edge of the joint (at  $y = +c$ ) would have a higher value of shear stress than the other side (at  $y = -c$ ).

As previously discussed, the adhesive stress component  $\tau_{yz}^a$  was said to be small enough so that it can be neglected. To justify this statement, the peak values of  $\tau_{yz}^a$  are calculated using equation

(25) and compared with the peak values of  $\tau_{xz}^a$ . For this example problem, the peak values of  $\tau_{yz}^a$  occur along  $x = a/2$  since this is the location where the maximum gradient in the load function, given by equation (26), exists. In order to calculate  $\tau_{yz}^a$ , the stress resultant  $N_y$  must be known. Using equations (15) and (26), and assuming  $N_y$  to be zero at  $y = 0$ ,  $N_y$  at  $x = a/2$  can be determined to be

$$N_y = 4.38 \frac{\pi}{a} y \quad (29)$$

Using the tension-loaded joint solution described in Appendix A, and for the boundary conditions  $\sigma_y^o = 0$  at  $y = -c$ , and  $\sigma_y^o = N_y(c)/t_o$  at  $y = c$ , an expression describing the  $N_y$  contribution to the  $\tau_{yz}^a$  stress is determined.

$$\left(\tau_{yz}^a\right)_{N_y} = t_o \frac{F_1}{\lambda_o^2} + t_o \lambda_o \left[ \frac{N_y(c)}{2t_o} \cdot \frac{\sinh \lambda_o y}{\cosh \lambda_o c} + \left( \frac{N_y(c)}{2t_o} - \frac{F_1 c}{\lambda_o^2} \right) \frac{\cosh \lambda_o y}{\sinh \lambda_o c} \right] \quad (30)$$

where  $\lambda_o$  is given by equation (A2), and

$$F_1 = \frac{G_a}{t_a E_y t_o t_i} \cdot \frac{dN_y}{dy} \quad (31)$$

Profiles of  $\left(\tau_{yz}^a\right)_{N_{xy}}$ ,  $\left(\tau_{yz}^a\right)_{N_y}$ , and the total solution for  $\tau_{yz}^a$ , as expressed by equations (24), (30), and (25), respectively, are plotted in Figure 15 for the glass/epoxy joint case. It is clear that in order to obtain an accurate prediction for  $\tau_{yz}^a$ , both components contributing to equation (25) must be included. Ignoring one contribution can result in a dramatic departure from the total  $\tau_{yz}^a$  solution, as well as result in a  $\tau_{yz}^a$  stress prediction which violates assumption (2) of the derivation. The validity of this last statement can be confirmed by computing the  $\left(\tau_{yz}^a\right)_{N_{xy}}$  and  $\left(\tau_{yz}^a\right)_{N_y}$  stresses with reference to the inner adherend stresses  $\tau_{xy}^i$  and  $\sigma_y^i$ , respectively. In order

for assumption (2) to hold, the adhesive stress profiles predicted relative to the inner and outer adherends must be identical to each other. This result is only achieved for the total solution, as expressed by equation (25).

Finally, a comparison shows that the maximum value of  $\tau_{yz}^a$  in Figure 15 is only 9% of the peak value of  $\tau_{xz}^a$  in Figure 14, despite the high gradient of  $N_{xy}$  in the  $x$ -direction. This confirms the previously made statement that the  $\tau_{yz}^a$  stress component is small relative to  $\tau_{xz}^a$  and can usually be neglected.

### **Validation by Finite Element Analysis**

Further validation of the closed form solution is demonstrated by comparison of the adhesive shear stress predicted by equation (23) with FEA results. Consider the system shown in Figure 16. Here a lap-jointed aluminum panel of dimensions, support, and loading configuration shown in the figure produces a region of approximately uniform shear stress resultant  $N_{xy}$  away from the free edge. The overlap dimension of the panel is  $2c = 12.7$  mm, the adherends have thickness  $t_i = t_o = 1.016$  mm, and the bondline thickness is  $t_a = 0.508$  mm. The Young's modulus of the aluminum is 68.9 GPa, and the shear modulus of the adhesive is  $G_a = 1.46$  GPa. Also in Figure 16 is the FEA mesh used for analysis. Note that solid elements needed to be used in modeling the joint due to the nature of applying shear loading to a lap joint geometry. In contrast, tension-loaded joints can often be analyzed using two-dimensional FEA models.

The applied load  $F = 623$  N was chosen such that a theoretically constant (by simple Strength of Materials calculation) shear flow in the web of 17.5 N/mm exists. The FEA prediction of  $N_{xy}$ ,

plotted in Figure 16 as a function of the  $x$ - and  $y$ -directions, reveals that the actual average shear flow is 18.7 N/mm, and is approximately constant over the hatched region (see Figure 16) away from the free edge. This value of  $N_{xy} = 18.7$  N/mm is used as the loading for the closed form prediction of adhesive shear stress (Equation 23) along the path A-B indicated in Figure 16. Figure 17 plots the FEA and closed form predictions of  $\tau_{xz}^a$  along path A-B. The closed form solution over-predicts the peak shear stress by less than 2%. It is clear from the comparison shown in Figure 17 that the closed form solution provides an accurate prediction of adhesive shear stress. Additionally, the closed form equations provided a solution at much less computational cost than FEA.

## 5. Solution for Finite Case

The previous section treated the case of a semi-infinite joint subjected to a gradient loading. In this section, a closed form solution of the governing equation (11) is presented for the case of a finite sized doubler bonded to a base structure that is subjected to remotely applied in-plane shear loading, as shown in Figure 2b. A doubler is often bonded onto a structure to serve as a reinforced hard point for component attachment, such as an antenna on an aircraft fuselage, or to increase thickness at local areas for carrying loads through holes, e.g. a bolted attachment. In this case, the bonded doubler patch can be considered as the outer adherend, and the plate to which it is adhesively joined, the inner adherend. Since the doubler is finite in size along both the  $x$ - and  $y$ -axes, a simple solution approach can not be employed such that the governing equation can be treated as an ordinary differential equation. Here the full partial differential equation must be solved. The rectangular bonded doubler is a particular configuration for which an assumed  $\tau_{xy}^o$  stress function can be chosen to satisfy both the boundary conditions of the problem ( $\tau_{xy}^o = 0$

at  $x = 0, a$  and  $y = 0, b$ ) and the governing equation. A double Fourier sine series satisfies both of these conditions.

$$\tau_{xy}^o = \sum_{m=1}^{\infty} \sum_{n=1}^{\infty} A_{mn} \sin \frac{m\pi x}{a} \sin \frac{n\pi y}{b} \quad (32)$$

The Fourier coefficient  $A_{mn}$  is determined such that the governing equation (11) is satisfied. To achieve this, the nonhomogeneous term of the governing equation,  $C_o$ , must also be represented by a double Fourier sine series.

$$C_o = \sum_{m=1}^{\infty} \sum_{n=1}^{\infty} C_{mn} \sin \frac{m\pi x}{a} \sin \frac{n\pi y}{b} \quad (33)$$

where  $C_{mn}$  is the Fourier coefficient in equation (33) and is calculated by

$$C_{mn} = \frac{4}{ab} \int_0^a \int_0^b C_o(x, y) \sin \frac{m\pi x}{a} \sin \frac{n\pi y}{b} dy dx \quad (34)$$

In equation (34), the term  $C_o(x, y)$  within the double integral is the nonhomogeneous term of the governing equation (11), and should not to be confused with the  $C_o$  on the left hand side of equation (33). Note that spatially varying  $N_{xy}(x, y)$  loading is accounted for through the  $C_o(x, y)$  term in equation (34). For non-constant  $N_{xy}$ , the necessary  $N_x$  and  $N_y$  stress resultants can be determined from the plate equilibrium equations (14) and (15) in a manner similar to that presented in the previous section.

Inserting equations (32) and (33) into the governing equation (11), the Fourier coefficient of equation (32) can now be solved for.

$$A_{mn} = \frac{C_{mn}}{\left(\frac{\pi m}{a}\right)^2 + \left(\frac{\pi n}{b}\right)^2 + \lambda^2} \quad (35)$$

The series solution given by equation (32) provides the in-plane shear stress distribution within the outer adherend. The adhesive shear stress components,  $\tau_{xz}^a$  and  $\tau_{yz}^a$ , are calculated using

equations (2) and (3). Note that in the finite sized joint case, the  $\tau_{yz}^a$  stress is significant in magnitude at two opposing doubler boundaries  $x = 0$  and  $x = a$ , even for a constant  $N_{xy}$  applied load.

### Example and Applications

An example calculation is now presented. Consider a thin glass/epoxy structure (inner adherend) carrying shear load. A carbon/epoxy doubler (outer adherend) is bonded to the structure. The geometry of this example problem is listed in Table II. The material properties used in the calculation are taken from Table I. Applied shear load is a constant  $N_{xy} = 17.5$  N/mm.

Table II. Finite-Sized Doubler Geometry

Doubler Parameter	Symbol	Value
length of doubler in $x$ -direction	$a$	127 mm
length of doubler in $y$ -direction	$b$	76.2 mm
inner adherend thickness; glass/epoxy base structure	$t_i$	1.27 mm
outer adherend thickness; carbon/epoxy doubler	$t_o$	2.54 mm
adhesive thickness	$t_a$	0.508 mm

The results of the calculation are shown by the three-dimensional stress surface plots in Figures 18 to 20. In Figure 18, the in-plane shear stress  $\tau_{xy}^o$  in the doubler is plotted. The plots correctly show that this stress goes to zero at the boundaries. Away from the edges, towards the center of the doubler, the stress is the average shear stress, 5.97 MPa, as calculated by equation (27). The adhesive shear stress component  $\tau_{xz}^a$ , plotted in Figure 19, has maximum magnitude at two opposing edges of the doubler, at  $y = 0$  and  $y = b$ . Similarly, the adhesive shear stress component  $\tau_{yz}^a$  is maximum at the edges  $x = 0$  and  $x = a$ , as shown in Figure 20.

These plots were generated for a large number of terms ( $m = 167, n = 101$ ) taken in the series solution, equation (32). A drawback to the sine series solution applied to this problem is that convergence can be slow. This is especially so when the gradients in  $\tau_{xy}^o$  occur at a length scale that is small compared with the overall size of the doubler, (e.g. less than one-tenth size). Figure 18 shows this to be the case for this example problem. Consequently a high number of terms in equation (32) needs to be used in order to converge upon an accurate solution. Table III lists values of peak adhesive shear stress for combinations of the number of terms taken in the double sine series solution. Values of  $(\tau_{xz}^a)_{\max}$  were taken at the location  $x = a/2, y = 0$ , and  $(\tau_{yz}^a)_{\max}$  values were taken at  $x = 0, y = b/2$ .

Table III. Convergence of Double Sine Series Solution; Units are in MPa

n	41		101		167		501	
m	$(\tau_{xz}^a)_{\max}$	$(\tau_{yz}^a)_{\max}$	$(\tau_{xz}^a)_{\max}$	$(\tau_{yz}^a)_{\max}$	$(\tau_{xz}^a)_{\max}$	$(\tau_{yz}^a)_{\max}$	$(\tau_{xz}^a)_{\max}$	$(\tau_{yz}^a)_{\max}$
41	6.74	5.76	7.69	5.75	7.96	5.75	8.24	5.75
101	6.70	7.21	7.65	7.19	7.92	7.19	8.20	7.19
167	6.70	7.66	<u>7.64</u>	<u>7.64</u>	7.90	7.63	8.18	7.63
501	6.70	8.13	7.64	8.10	7.91	8.09	8.19	8.09

The table shows that increasing the number of terms taken in  $m$  yields more accuracy in predicting  $(\tau_{yz}^a)_{\max}$ , while an increasing number of terms taken in  $n$  yields a more accurate prediction of  $(\tau_{xz}^a)_{\max}$ . This is due to the number of  $m$  and  $n$  terms each directly improving the representation of the doubler in-plane shear stress in the  $x$ - and  $y$ -directions, respectively, from

which  $(\tau_{yz}^a)_{\max}$  and  $(\tau_{xz}^a)_{\max}$  are computed. Obviously a better representation of  $\tau_{xy}^o$  in the  $x$ -direction (more  $m$  terms) would result in an improved calculation of  $\tau_{yz}^a$ . Similar statements can be made regarding  $\tau_{xz}^a$  and the number of  $n$  terms. Note that a higher predicted value of  $(\tau_{yz}^a)_{\max}$  is calculated for a combination of  $m = 501, n = 41$  than for  $m = 501, n = 501$ . This is due to the nature of the assumed sine series solution which predicts an oscillation of the  $\tau_{yz}^a$  stress about a mean value when plotted versus  $y$  at any station in  $x$  (e.g. at  $x = 0$ ) for a given number of terms taken in  $m$ . Shown in Figure 21, increasing the number of terms taken in  $n$  results in a convergence to that mean value (i.e. higher frequency yields lower amplitude), while changing the number of terms taken in  $m$  will change the mean value, as is reflected in Table III. The same arguments apply to explain this apparent loss of accuracy when comparing values of  $(\tau_{xz}^a)_{\max}$  for  $m = 41, n = 501$  with  $(\tau_{xz}^a)_{\max}$  calculated for  $m = 501, n = 501$ . Note that these differences, as listed in Table III, are negligible at less than 1% for the number of terms used in constructing this convergence study. However they would be higher if a lower number of  $m$  and  $n$  terms were taken, e.g.  $m = 21$  (see Figure 21).

The underlined values in Table III indicate the solution from which the plots in Figures 18 to 20 are constructed, i.e. at  $m = 167, n = 101$ . These values for  $m$  and  $n$  were chosen such that roughly ten half-sine waves fit within the edge boundary zone,  $\delta$ , where gradients in  $\tau_{xy}^o$  exist. The size of this boundary zone is indicated in Figure 18. A calculation of the boundary zone size,  $\delta$ , can be made using the relationship

$$\delta = -\frac{\ln \varepsilon}{\lambda} \quad (36)$$

where  $\lambda$  is given by equation (12), and  $\varepsilon$  is an arbitrarily chosen small tolerance value close to zero, e.g. use  $\varepsilon = 0.01$ . Equation (36) is derived from the general form of the semi-infinite joint solution, which assumes  $\tau_{xy}^o \propto e^{-\lambda x}$ .

In regions away from the corners of the doubler, the adhesive shear stress profiles for  $\tau_{xz}^a$  and  $\tau_{yz}^a$  can be accurately predicted using the semi-infinite joint solution approach presented in the previous section. The validity of performing such a calculation can be verified by observing the  $\tau_{xz}^a$  adhesive stress profile in Figure 19. In the regions away from the two opposing doubler boundaries,  $x = 0$  and  $x = a$ , the stress profile  $\tau_{xz}^a$  is only a function of  $y$ . Furthermore, this profile is identical to that which would be predicted by a semi-infinite joint calculation. To compute the  $\tau_{xz}^a(y)$  adhesive shear stress profile, away from the edges  $x = 0$  and  $x = a$ , the boundary conditions,  $\tau_{xy}^o = 0$  at  $y = 0$  and  $y = b$ , must be applied to the assumed solution, equation (18), in order to solve for the coefficients  $A_o$  and  $B_o$ . Equation (2) is then used to compute the adhesive stress component acting in the  $x$ - $z$  plane.

$$\tau_{xz}^a(y) = \frac{C_o}{\lambda^2} \left[ (\cosh \lambda b - 1) \frac{\sinh \lambda y}{\sinh \lambda b} - \cosh \lambda y + 1 \right] \quad \text{for } \delta < x < (a - \delta) \quad (37)$$

Equation (37) can be rewritten for  $\tau_{yz}^a(x)$  by replacing  $y$  with  $x$ , and  $b$  with  $a$ .

$$\tau_{yz}^a(x) = \frac{C_o}{\lambda^2} \left[ (\cosh \lambda a - 1) \frac{\sinh \lambda x}{\sinh \lambda a} - \cosh \lambda x + 1 \right] \quad \text{for } \delta < y < (b - \delta) \quad (38)$$

These formulae both predict a peak magnitude of shear stress,  $(\tau_{xz}^a)_{\max} = (\tau_{yz}^a)_{\max} = 8.33$  MPa, at the same locations for which values listed in Table III were obtained. This peak magnitude of adhesive shear stress can be considered the exact value. Comparing this value with the  $m = 167$ ,  $n = 101$  case in Table III, the values listed there are 8% below the exact. The values of  $(\tau_{xz}^a)_{\max}$

and  $(\tau_{yz}^a)_{\max}$  for the  $m = 501, n = 501$  case are less than 3% below the exact value. A plot of equation (37) for the bonded doubler example, is compared in Figure 22 with the double sine series based stress prediction using equation (32) for the  $m = 167, n = 101$  case.

The stress  $\tau_{xy}^o$  in the interior region of the doubler away from the edges is a nominal value calculated by equation (27). For doublers of practical size, this nominal stress region is quite large compared to the boundary zone regions (see Figure 18). Consequently, a self equilibrating applied load, or geometry that perturbs the stress state within the confines of this nominal stress zone, would not affect the prediction of adhesive stresses at the doubler boundary (or visa versa). An example would be an antenna mount, or a hole serving as a bolted attachment point, as shown in Figure 23. A crack being repaired using an adhesively bonded patch, shown in Figure 24, would also fall under this condition, so long as the crack geometry is smaller than the patch overall dimensions, and the resulting perturbed stress state does not affect the nominal stress state in regions close to the patch boundaries. Note that a separate analysis must be performed to account for the effects of stress concentrations that arise due to the hole or crack geometry. Such a calculation is greatly simplified when it is not necessary to simultaneously account for the boundary stress gradients.

Figures 23 and 24 show biaxial tension loading in addition to applied shear stress resultants. As mentioned previously, the tensile (or compressive) loads can be accounted for by using a tension loaded bonded joint analysis, and superposing the results of this analysis with the stress states predicted by the applied shear loading.

## 6. Conclusions

A general treatment of an adhesively bonded lap joint, loaded by spatially varying in-plane shear stress resultants, has been presented. The resulting governing partial differential equation describes the in-plane shear stress in one of the adherends. Solution of this equation generally permits the calculation of two adhesive shear stress components,  $\tau_{xz}^a$  and  $\tau_{yz}^a$ . While analogous to the governing equation written for the tension loaded lap joint case, this equation differs in that it is inherently two-dimensional. Additionally, since the second order derivative terms of the equation can be represented by the Laplacian Operator,  $\nabla^2$ , the governing equation can be readily applied to solve bonded joint problems which are more suitably described by cylindrical coordinates (see Figure 5).

For a semi-infinite joint, a closed-form solution to the governing equation was obtained under the conditions that the applied loading varies smoothly in the direction across the width of the bonded joint (i.e. perpendicular to the overlapping direction). This closed-form solution has been verified to be accurate through comparison to a numerical finite difference solution of the governing differential equation. Two cases were considered, a joint with glass/epoxy composite adherends, and another with carbon/epoxy composite adherends; both joints having identical geometry. The more compliant glass/epoxy joint developed a higher magnitude of  $\tau_{xz}^a$  adhesive shear stress than the carbon/epoxy joint. In order to accurately compute the  $\tau_{yz}^a$  adhesive shear stress, both contributions to  $\tau_{yz}^a$  arising from the gradient in  $N_{xy}$  as well as the existence of an equilibrium-maintaining  $N_y$  stress resultant needs to be included. For the example presented, this  $\tau_{yz}^a$  stress component was shown to be small relative to  $\tau_{xz}^a$ , even when high a gradient in  $N_{xy}$  was present.

A closed-form solution for a finite sized bonded doubler was obtained using a double sine series approximation. For this case, both the  $\tau_{xz}^a$  and  $\tau_{yz}^a$  adhesive shear stress components are significant. In order to achieve an accurate sine series based solution, the minimum number of terms taken in the series should be such that at least five sine wave oscillations exist within the length scale over which gradients in the doubler shear stress exists. Alternatively, an approximate, yet accurate, prediction of the maximum values of  $\tau_{xz}^a$  and  $\tau_{yz}^a$  stresses occurring at the boundaries of the doubler can be determined by treating the finite-sized doubler as semi-infinite. While this solution excludes the corner regions of the doubler, the adhesive shear stresses are predicted to be zero at these locations, and thus the discrepancy of this solution is inconsequential.

In the finite sized doubler example calculation, a boundary zone at the edge of the doubler was shown to exist. This boundary zone is the edge-adjacent region in which gradients in  $\tau_{xy}^o$  are significant, and thus  $\tau_{xz}^a$  and  $\tau_{yz}^a$  are of significant magnitude. The size of this boundary zone is governed by the term  $\lambda$ , in equation (12). For stiffer adherends, or a thicker adhesive layer, the boundary zone would be larger. In the analogous tension-loaded joint case, this  $\lambda$  term would contain the Young's Modulus of the adherends, which in general is several times larger (at least for isotropic materials) than the shear modulus. Therefore the boundary zone would typically be larger for the tension loaded case than the shear loaded case. Finally, when numerically modeling the joint, either by Finite Difference or Finite Element techniques, knowledge of  $\lambda$  aids in determining what node spacing is adequate enough to accurately resolve gradients in the bond stresses.

In the interior region of the doubler, confined by the boundary zone, the adhesive stresses are null, and the doubler in-plane stress,  $\tau_{xy}^o$ , is a nominal value which depends only on the magnitude of the remote applied loading,  $N_{xy}$ , and the relative stiffness of the adherends. Within this nominal stress zone, geometric features can exist (or self-equilibrating loads applied), such as a crack in the base structure (inner adherend), or a hole passing through both adherends. If these features are such that the resulting perturbed stress field surrounding the feature is within the confines of the nominal stress zone, then the two problems of predicting the doubler edge stresses, and the stresses arising due to the geometric feature, can be treated independently. That is, they would not influence each other, thus greatly simplifying their individual treatment.

The analysis presented, while two dimensional, is similar enough to the tension-loaded case to be familiar, and remains simple in form. The solution presented is applicable to several joint geometries and applications. Additionally, since the analysis is linear, a joint under simultaneous biaxial tension and shear loading can be now treated by superposing the results of separate tension and shear loaded analytical solutions. Failure prediction within the adhesive would then need to account for this multi-component field of adhesive shear stress. There exists yet many geometries for which a closed-form solution is not possible. However, most of these problems can still be solved numerically since the governing partial differential equation that was derived is well suited for solution techniques based on the Finite Difference method.

## References

- [1] Hart-Smith, L. J. and Strindberg, G., *Proc. Institution of Mechanical Engineers* **211 Part G**, 133-156 (1997).
- [2] van Rijn, L. P. V. M., *Composites Part A* **27A**, 915-920 (1996).

- [3] Hart-Smith, L. J., Adhesive-Bonded Single-Lap Joints, NASA-Langley Contract Report NASA-CR-112236 (1973).
- [4] Hart-Smith, L. J., Adhesive-Bonded Double-Lap Joints, NASA-Langley Contract Report NASA-CR-112235 (1973).
- [5] Volkersen, O., *Luftfahrtforschung* **15**, 41-47 (1938).
- [6] Goland, M. and Reissner, E., *J. of Applied Mechanics* **11**, A17-A27 (1944).
- [7] Oplinger, D. W., *Int. J. Solids Structures* **31**, No. 12, 2565-2587 (1994).
- [8] Tsai, M. Y., Oplinger, D. W., and Morton, J., *Int. J. Solids Structures* **35**, No. 12, 1163-1185 (1998).
- [9] Engineering Sciences Data Unit. Stress Analysis of Single Lap Bonded Joints. Data Item 92041 (1992).
- [10] Adams, R. D. and Peppiatt, N. A., *J. Adhesion* **9**, 1-18 (1977)
- [11] Bruhn, E. F., *Analysis and Design of Airplane Structures* (self copyright, Cincinnati, 1949) Chap. C8, pp. C8.1-C8.18, and Chap. C9, pp. C9.1-C9.26.
- [12] Popov, E. P., *Engineering Mechanics of Solids* (Prentice Hall, New Jersey, 1990) Chap. 7, pp. 357-402.
- [13] Flügge, W., *Stresses in Shells* (Springer-Verlag, New York, 1973), pp. 61.
- [14] Grossmann, S. I. and Derrick, W. R., *Advanced Engineering Mathematics* (Harper & Row, New York, 1988), pp. 86-87.
- [15] Hart-Smith, L. J., *Joining of Composite Materials* ASTM STP 749, 3-31 (1981).

## Acknowledgements

Deserved acknowledgement is to be given to Larry Ilcewicz and Don Oplinger of the Federal Aviation Administration, John Tomblin of Wichita State University, and Dieter Koehler and Todd Bevan of Lancair for their assistance, guidance, and funding which made this research possible.

## Appendix A. Tension-Loaded Lap Joint Solution

For the tension-loaded lap joint, as depicted in Figure 1, a simple closed-form solution has been developed based on shear lag theory [5]. The governing equation for this problem is

$$\frac{d^2 \sigma_y^o}{dy^2} - \lambda_o^2 \sigma_y^o + D_o = 0 \quad (\text{A1})$$

$$\text{where } \lambda_o^2 = \frac{G_a}{t_a} \left( \frac{1}{E_y^o t_o} + \frac{1}{E_y^i t_i} \right) \text{ and } D_o = \frac{G_a}{t_a} \cdot \frac{N_y}{E_y^i t_i t_o} \quad (\text{A2) and (A3)}$$

The solution of the governing equation (A1) yields the outer adherend tensile stress

$$\sigma_y^o = \frac{\cosh \lambda_o y \left( \frac{N_y}{2t_o} - \frac{D_o}{\lambda_o^2} \right) + \frac{\sinh \lambda_o y}{\sinh \lambda_o c} \frac{N_y}{2t_o} + \frac{D_o}{\lambda_o^2}}{\cosh \lambda_o c} \quad (\text{A4})$$

The adhesive shear stress, due to  $N_y$  loading, can be calculated from (A4).

$$\left( \tau_{yz}^a \right)_{N_y} = t_o \frac{d\sigma_y^o}{dy} = t_o \lambda_o \left[ \frac{\sinh \lambda_o y \left( \frac{N_y}{2t_o} - \frac{D_o}{\lambda_o^2} \right) + \frac{\cosh \lambda_o y}{\sinh \lambda_o c} \frac{N_y}{2t_o}}{\cosh \lambda_o c} \right] \quad (\text{A5})$$

This solution is for the geometry shown in Figure 1, where the joint has length  $2c$  and the boundary conditions are

$$\sigma_y^o = 0 \text{ at } y = -c \quad (\text{A6})$$

$$\sigma_y^o = \frac{N_y}{t_o} \text{ at } y = c \quad (\text{A7})$$

Furthermore, the solution is for the case of loading which is constant in the  $y$ -direction. When the load has a gradient in  $y$ , the *Method of Undetermined Coefficients* [14] can be used to solve the governing equation (A1). This method is described in detail in Appendix B.

## Appendix B. Method of Undetermined Coefficients

The *Method of Undetermined Coefficients* is a standard method [14] by which the particular solution to a nonhomogeneous ordinary differential equation (ODE) is determined. Consider a second order ODE, similar to the form of the equation governing bonded joint behavior.

$$\frac{d^2\psi}{dy^2} - \lambda^2\psi + F(y) = 0 \quad (\text{B1})$$

The homogeneous solution to equation (B1) is

$$\psi_H(y) = A \cosh \lambda y + B \sinh \lambda y \quad (\text{B2})$$

where  $A$  and  $B$  are arbitrary constants. The method presented can predict the particular solution when the nonhomogeneous term  $F(y)$  has one of three forms: i) an  $n^{\text{th}}$  order polynomial, ii) the product of a polynomial with an exponential function, or iii) the product of a polynomial with an exponential function and a sine or cosine function. The case of the  $F(y)$  being a second order polynomial is presented as an example to demonstrate the method.

Let  $F(y)$  be represented by a general second order polynomial.

$$F(y) = F_o + F_1 y + F_2 y^2 \quad (\text{B3})$$

A particular solution can be assumed to have the form

$$\psi_p(y) = a_o + a_1 y + a_2 y^2 \quad (\text{B4})$$

By inserting equations (B3) and (B4) into the nonhomogeneous ODE (B1),

$$2a_2 - \lambda^2(a_o + a_1 y + a_2 y^2) + F_o + F_1 y + F_2 y^2 = 0 \quad (\text{B5})$$

and comparing coefficients of like powers of the independent variable,

$$y^0: \quad 2a_2 - \lambda^2 a_o + F_o = 0 \quad (\text{B6})$$

$$y^1: \quad -\lambda^2 a_1 + F_1 = 0 \quad (\text{B7})$$

$$y^2: \quad -\lambda^2 a_2 + F_2 = 0 \quad (\text{B8})$$

equations (B6 to B8) can be solved to determine the coefficients of (B4).

$$a_o = \frac{1}{\lambda^2} \left( \frac{2F_2}{\lambda^2} + F_o \right), \quad a_1 = \frac{F_1}{\lambda^2}, \quad \text{and} \quad a_2 = \frac{F_2}{\lambda^2} \quad (\text{B9 to B11})$$

The total solution is the sum of the homogeneous (B2) and particular (B4) solutions.

$$\psi(y) = \psi_H(y) + \psi_p(y) = A \cosh \lambda y + B \sinh \lambda y + \frac{1}{\lambda^2} \left( \frac{2F_2}{\lambda^2} + F_o \right) + \frac{F_1}{\lambda^2} y + \frac{F_2}{\lambda^2} y^2 \quad (\text{B12})$$

The constant terms  $A$  and  $B$  are determined from the boundary conditions. Note that a nonhomogeneous term  $F(y)$  of parabolic form is representative of the parabolic shear stress profile present in the shear web of an I-beam, as shown in Figure 7.

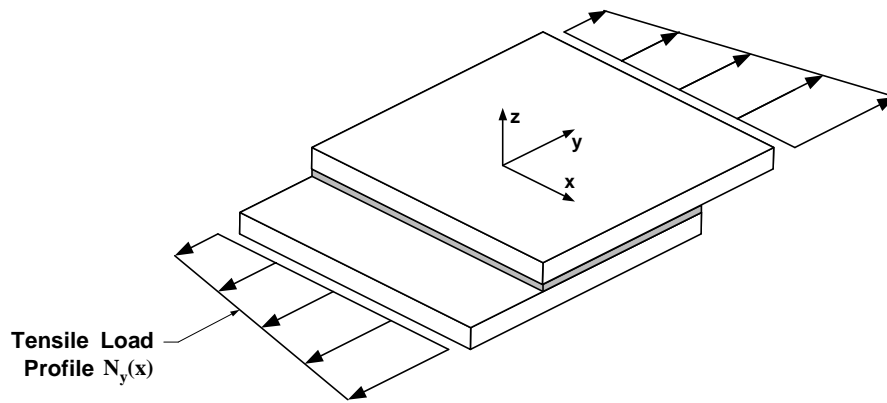
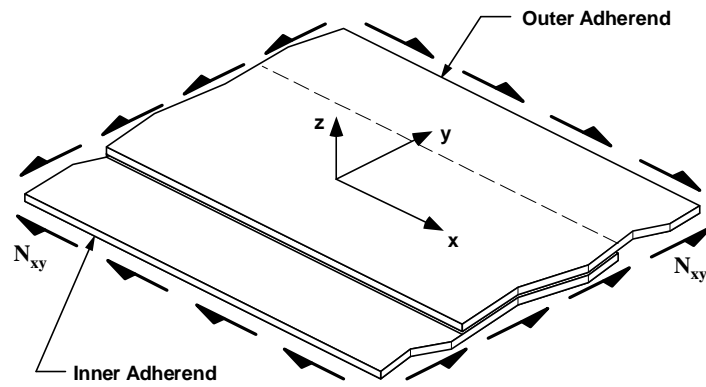
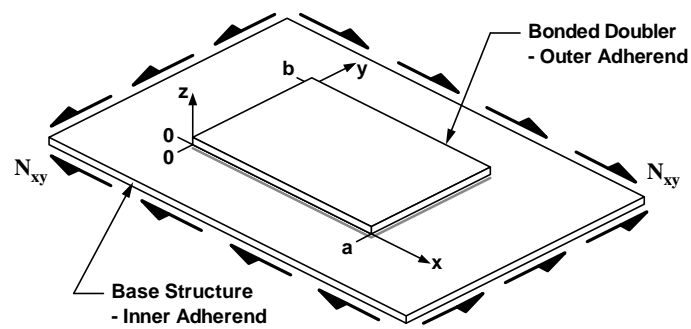


Figure 1. Tension Loaded Lap Joint



(a) Semi-Infinite Lap Joint



(b) Finite Sized Doubler Bonded onto Plate with Remote Shear Loading  $N_{xy}$

Figure 2. Adhesive Bonded Assemblies of Semi-Infinite and Finite Size

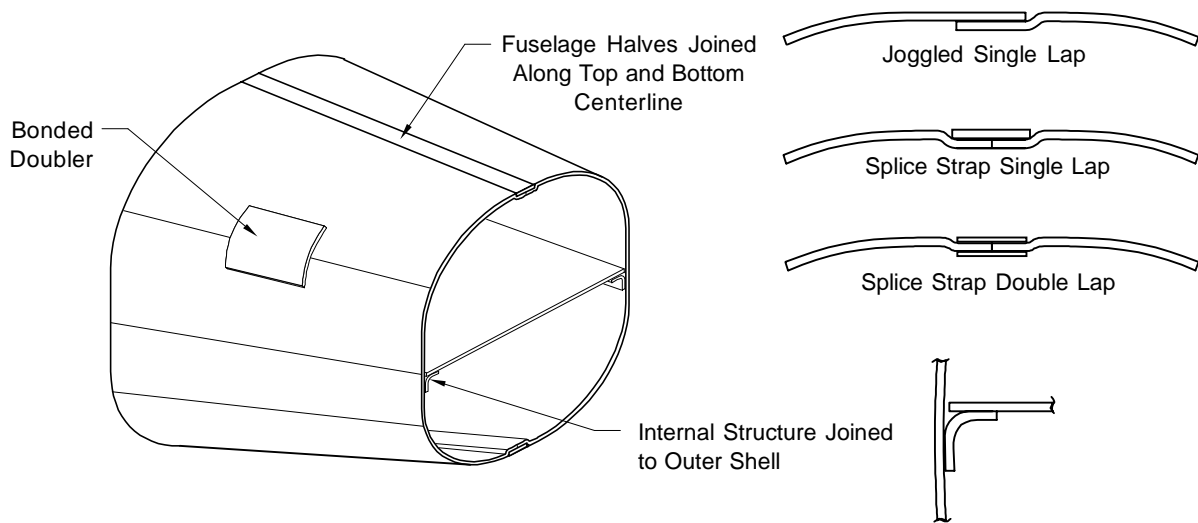
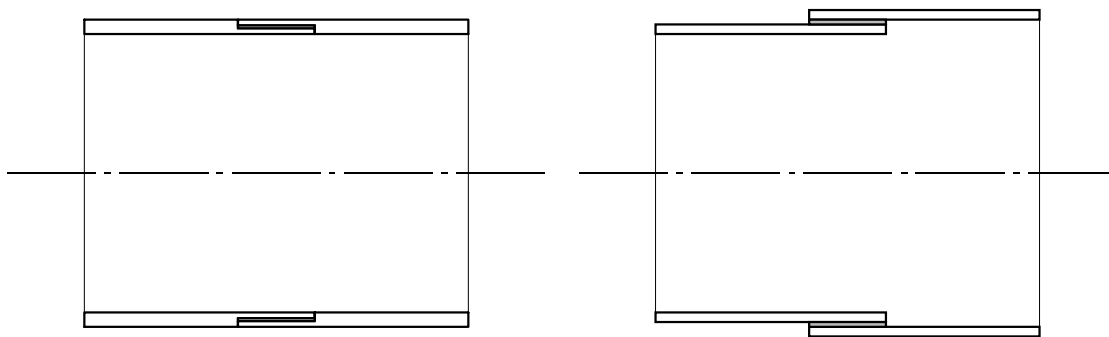
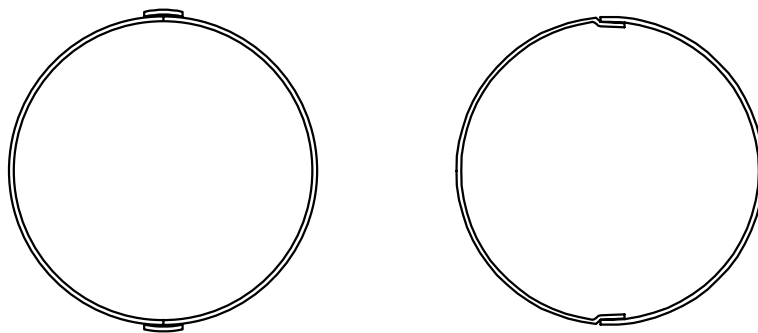


Figure 3. Typical Aft Section of Small Aircraft Bonded Fuselage



(a) Circumferential



(b) Longitudinal

Figure 4. Circumferential and Longitudinal Tubular Lap Joints

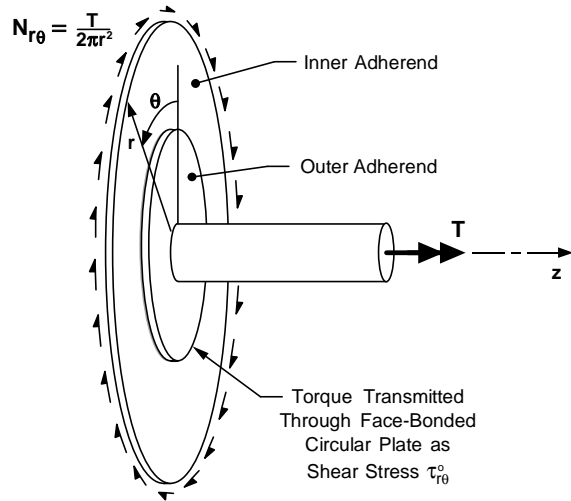


Figure 5. Torsion Loaded Circular Bonded Joint

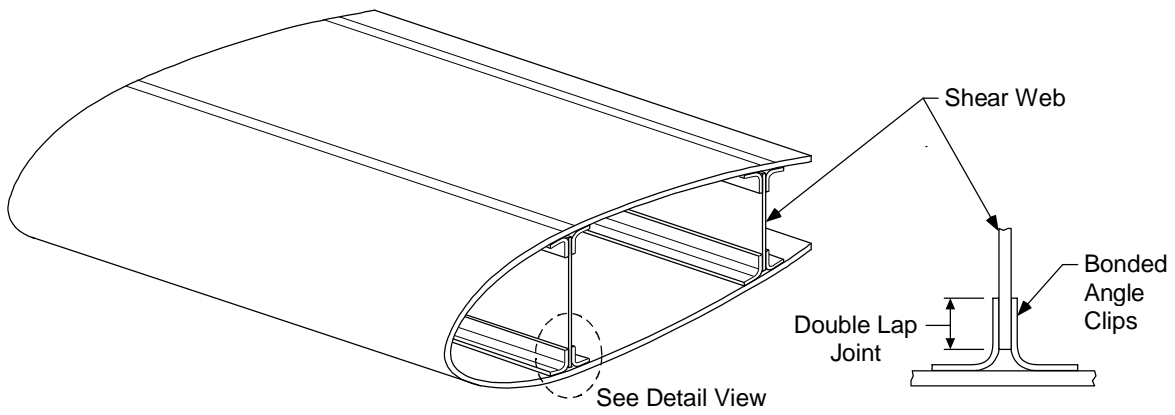


Figure 6. Shear Webs Forming Bonded Wing Box Assembly

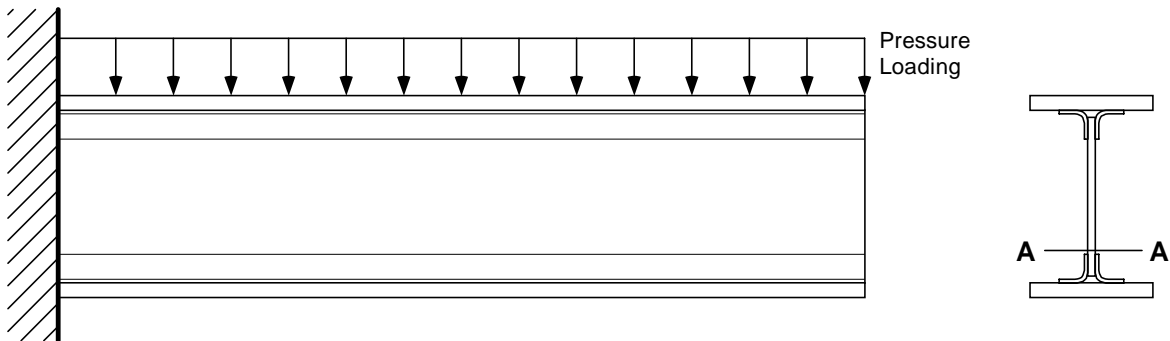


Figure 7. Constant Cross-Section I-Beam Under Uniform Pressure Load

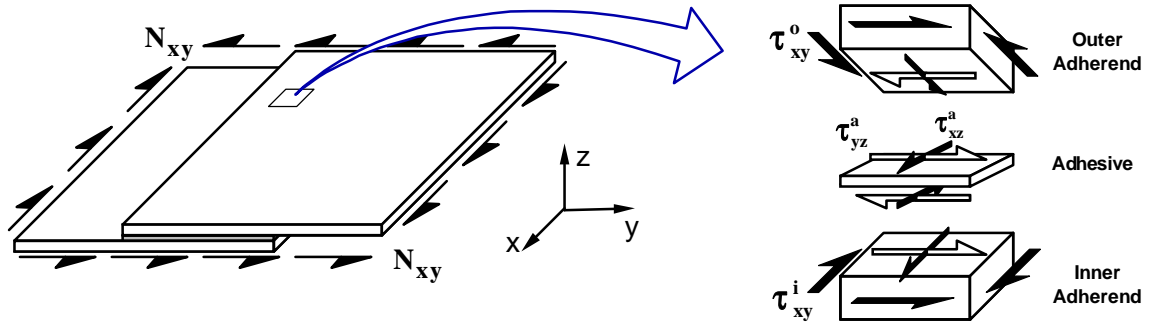


Figure 8. Lap Joint Bonded Shear Panel and Differential Element Showing Stresses in Adhesive and Adherends

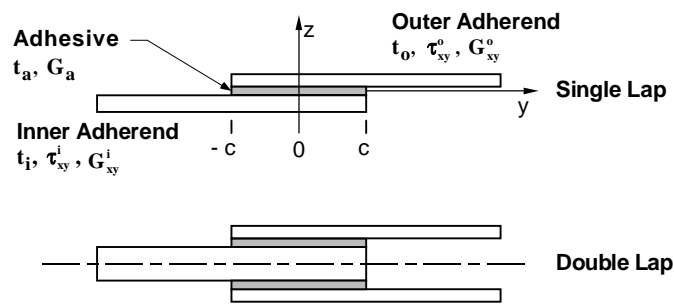


Figure 9. Single and Double Lap Joint Geometry

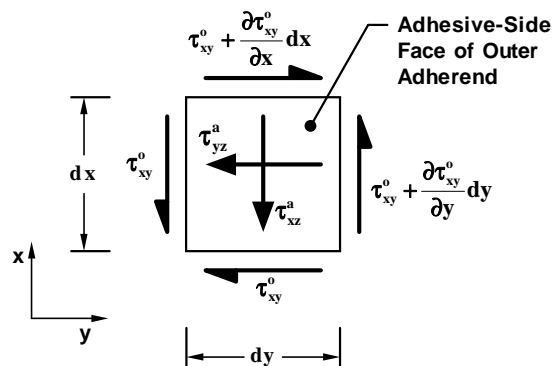


Figure 10. Adhesive and Adherend Stresses Acting on Differential Element of Outer Adherend

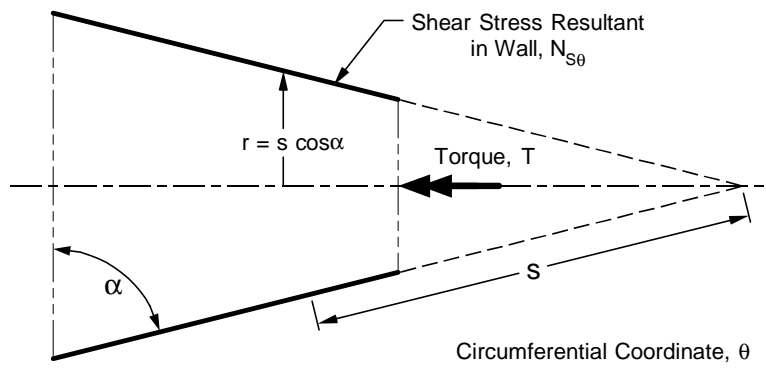


Figure 11. Conical Shell with Torsion Load

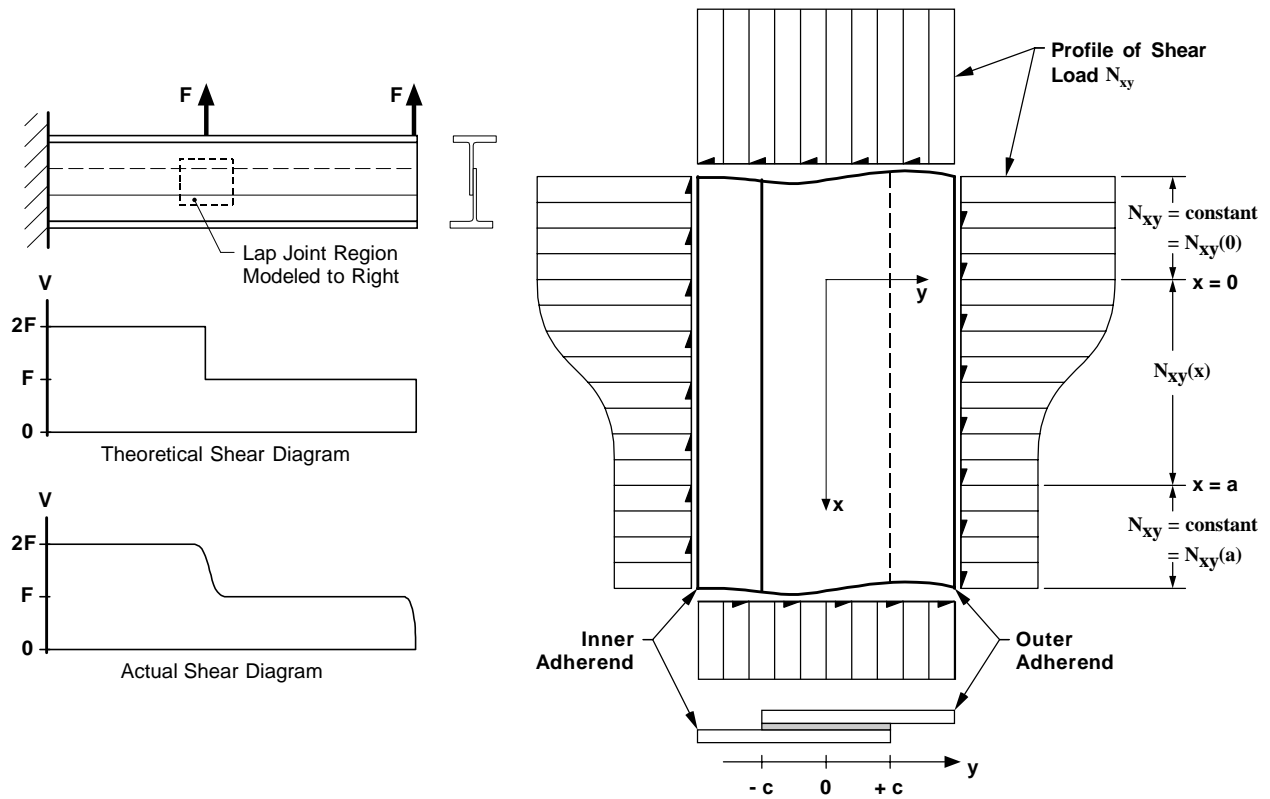


Figure 12. Lap Jointed Shear Web Under Spatially Varying Shear Load

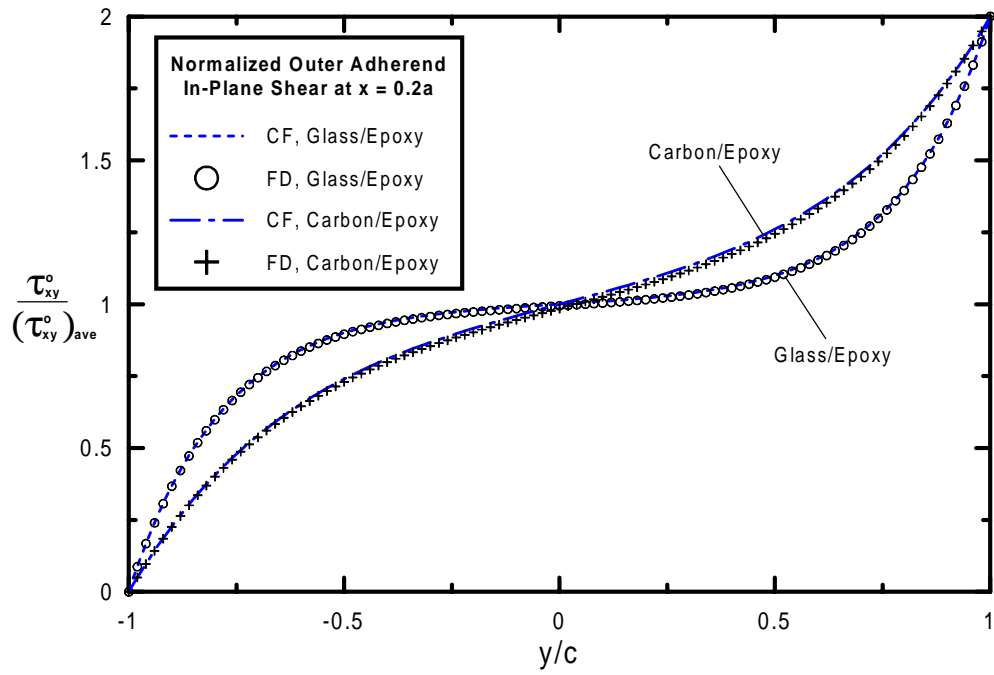


Figure 13.  $\tau_{xy}^o$  Adherend In-Plane Shear Stress,  $(\tau_{xy}^o)_{ave} = 3.28$  MPa

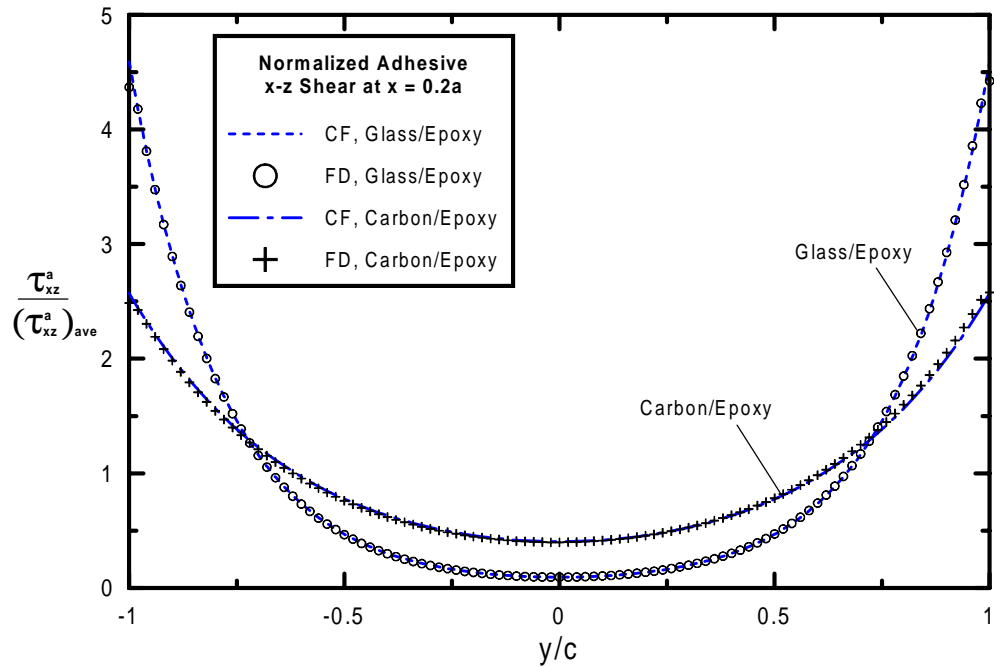


Figure 14.  $\tau_{xz}^a$  Adhesive Shear Stress,  $(\tau_{xz}^a)_{ave} = 1.31$  Mpa

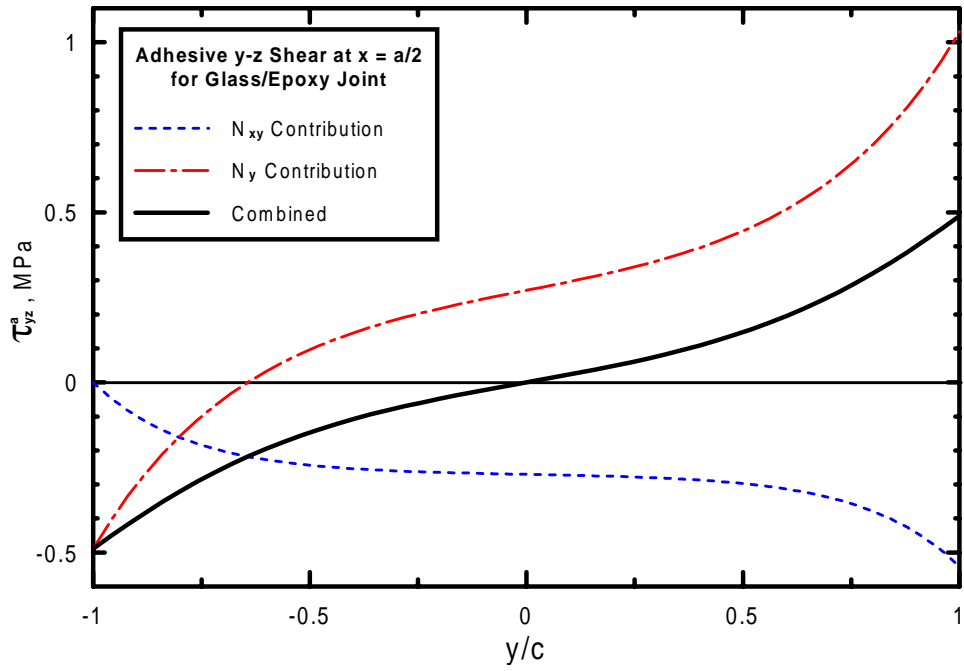


Figure 15.  $\tau_{yz}^a$  Adhesive Shear Stress for Glass/Epoxy Semi-Infinite Joint

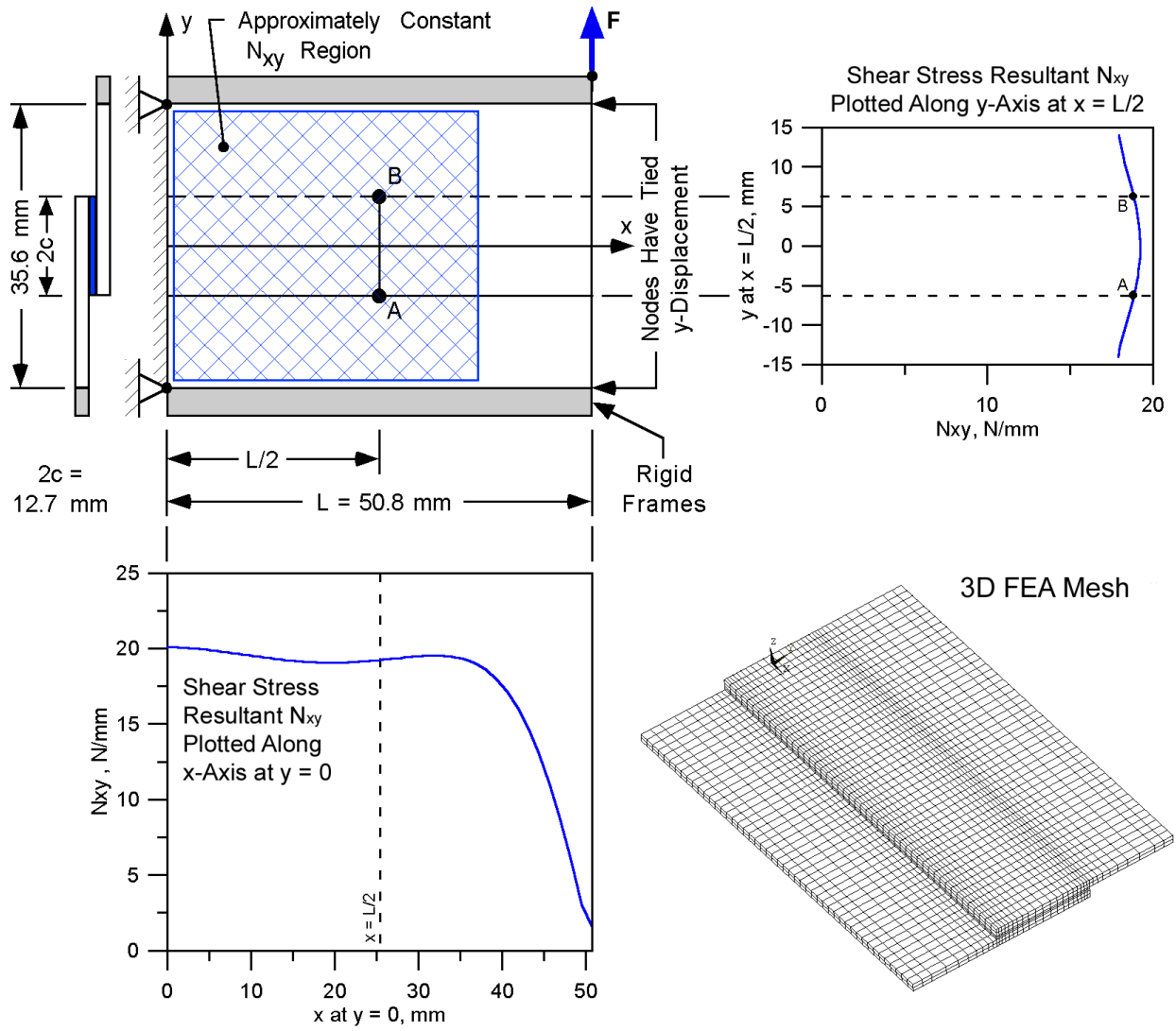


Figure 16. Shear Stress Resultant Profile in Lap-Jointed Aluminum Panel

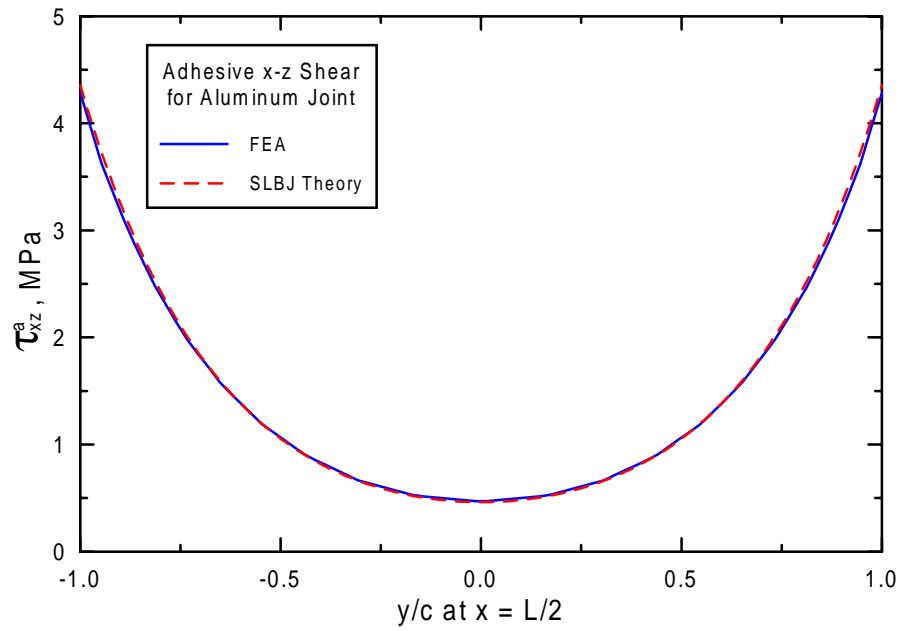


Figure 17. Comparison of Adhesive Shear Stress Predicted by FEA and Closed Form Solution;  $\tau_{xz}^a$  Plotted Along Path A-B in Figure 16.

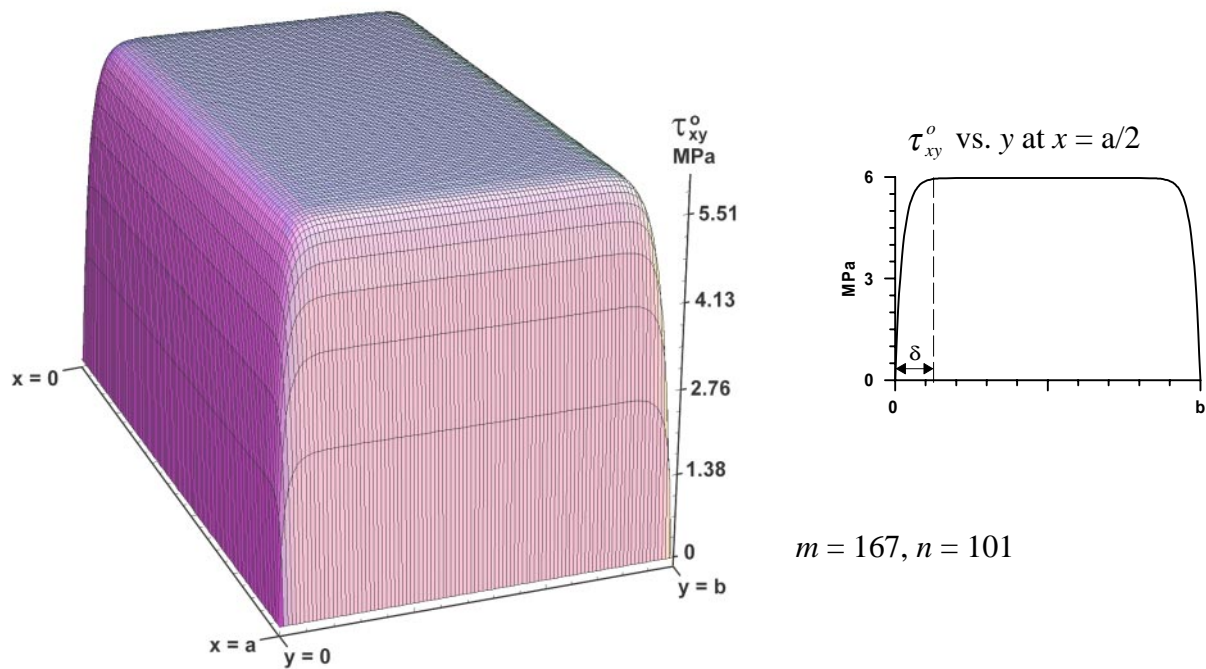


Figure 18. Adherend Shear Stress  $\tau_{xy}^o$  in Doubler

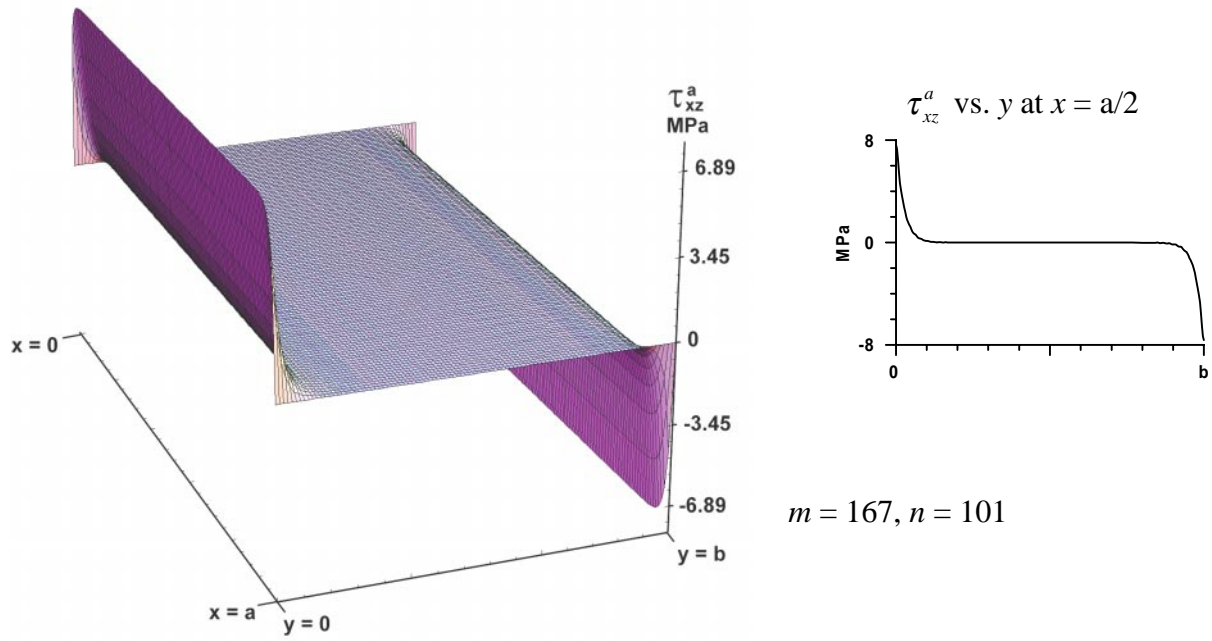


Figure 19. Adhesive Shear Stress  $\tau_{xz}^a$

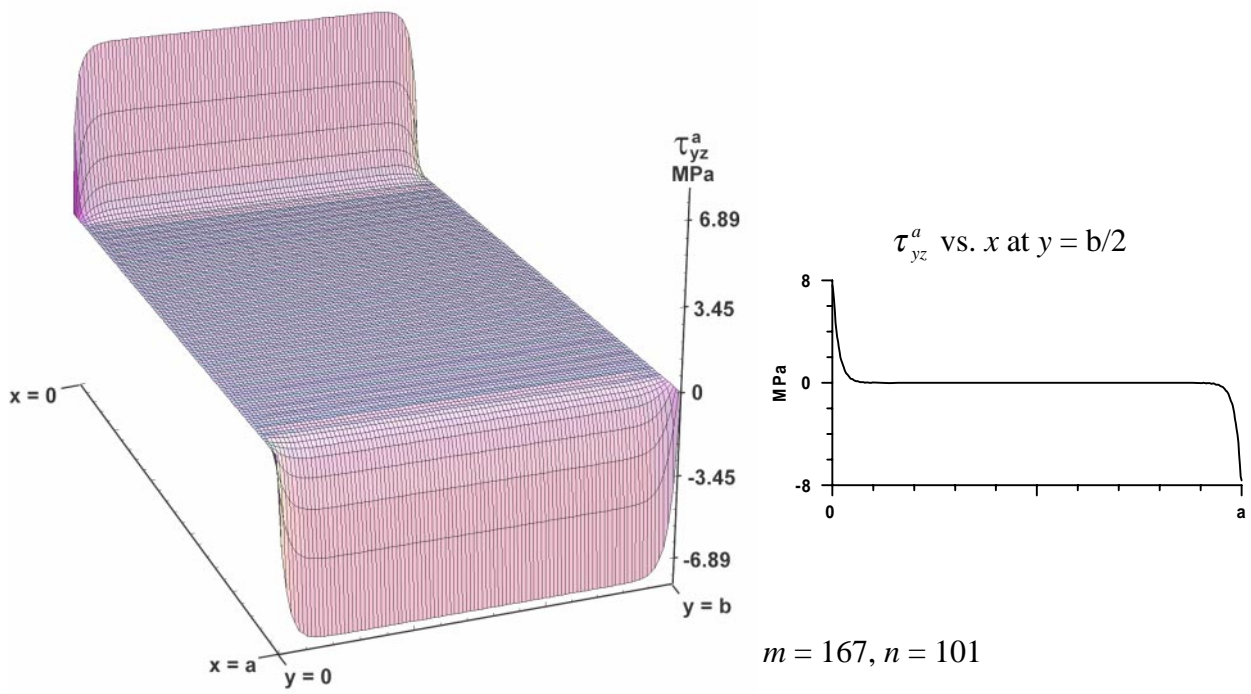


Figure 20. Adhesive Shear Stress  $\tau_{yz}^a$

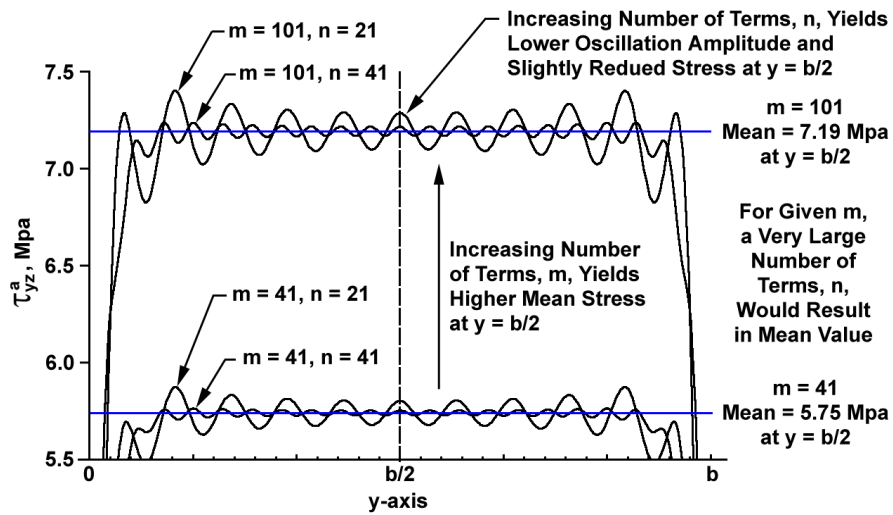


Figure 21. Oscillatory Profile of Adhesive Shear Stress  $\tau_{yz}^a$  at  $x = 0$  for Lower Numbers of Terms  $m$  and  $n$  Used in Infinite Series Solution

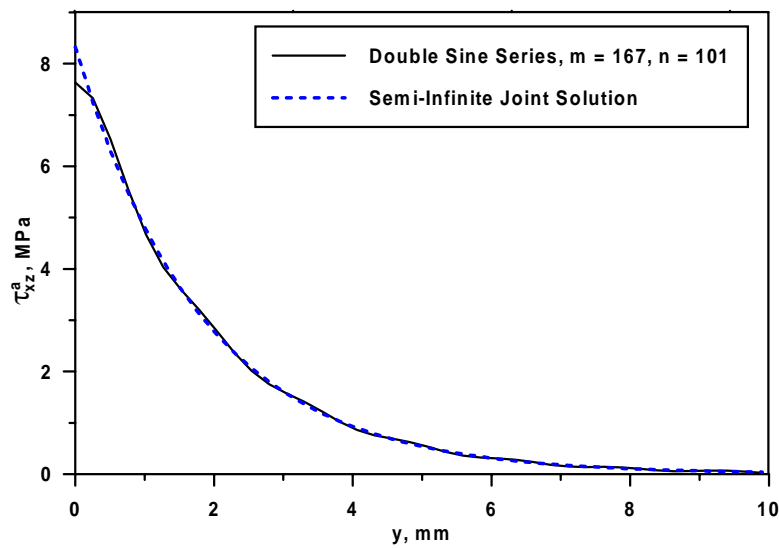


Figure 22. Comparison of Adhesive Shear Stress  $\tau_{xz}^a$  at  $x = a/2$  as Predicted by Double Sine Series and Semi-Infinite Joint Solutions

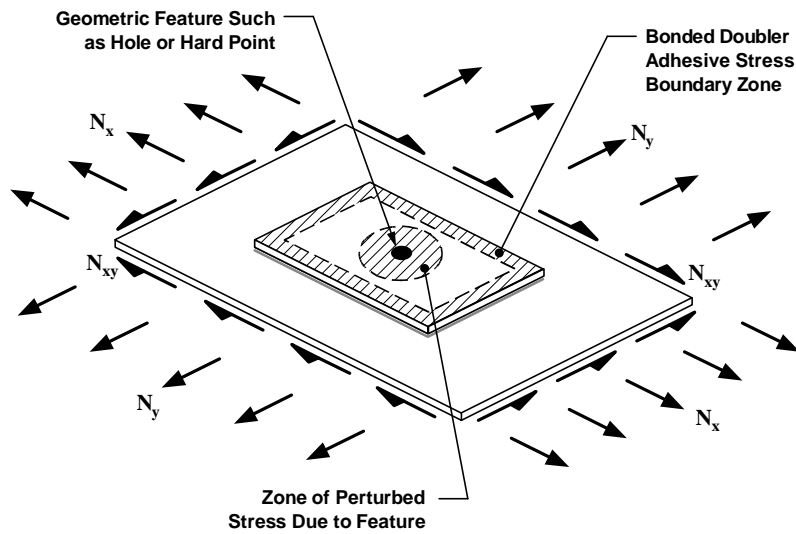


Figure 23. Bonded Doubler Applied to Reinforce Regions with Holes or Hard Points

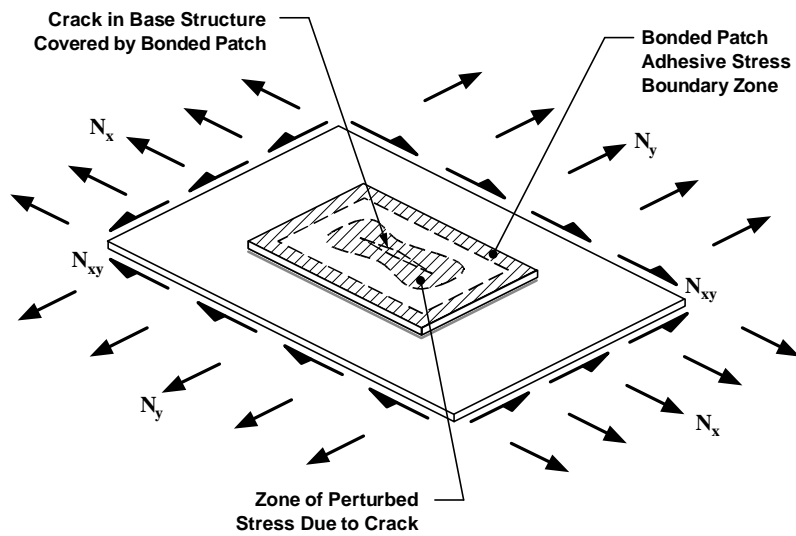


Figure 24. Crack Repair Using Bonded Patch